# Numerical simulation of high-temperature superconducting stacked-tape magnetic lens via H-$\phi$ model

Wenhao Li, Qing Zhang, M. D. Ainslie, *Senior Member*, *IEEE*, Difan Zhou, Jinyu He, Yibing Zhang and Chuanbing Cai

***Abstract*—Magnetic lens, exploiting the induced screening current, may concentrate the spatial magnetic flux. This concept has been realized by several research groups using GdBCO and/or $MgB_2$ bulk superconductors. The limitation of the magnitude of concentrated flux density lies on the mechanical brittleness of the materials and the flux instability. High-temperature superconducting (HTS) tape possesses excellent mechanical and flux pinning properties and hence is a good candidate for magnetic lens. In this study, we implemented numerical simulations on the design of magnetic lenses using HTS stacked tapes. The models were constructed based on H-$\phi$ formulations. We investigated and compared the concentration effect of various magnetic lenses with different topologies. The results show that a central field of 22.69 T and 25.62 T can be achieved respectively with rectangular-shaped stacks and X-shaped stacks in an applied magnetic field of 20 T. An optimized design of the magnetic lens has been proposed and correspondingly the mechanism for a better concentration-effect has been explained which provides a good reference for future experiments and applications.**

***Index Terms*—Superconducting tapes, Finite element methods, Magnetic shielding.**

## I. Introduction

HIGH and continuous magnetic fields are critical physical conditions for a wide range of medical and scientific research. Matsumoto and Kiyoshi *et al*. proposed the concept of the magnetic lens which exploits the diamagnetic shielding property of HTS materials to reshape the distribution of the external magnetic field and to concentrate the local magnetic flux density in the desired region [1]-[4]. Such a design can provide high and continuous central magnetic fields but requires no additional power consumption.

Zhang *et al*. achieved 11 T at the center of a GdBCO magnetic lens in an applied field of 5 T yielding a gain factor of 100% [5], [6]. They demonstrated that the mechanical fragmentation of the bulk magnetic lens and the occurrence of magnetic flux jumps are the biggest obstacles that limit the high-field application of the magnetic lens. Recently, Fujishiro *et al*. proposed a new concept of a hybrid trapped field magnetic lens, and its practicality has been shown experimentally [7]-[12].

HTS tape possesses many advantages in high-field applications. The very high tensile strength of the superalloy substrate ensures mechanical performance under high magnetic fields. The silver stabilization layer on top of the HTS tape helps dissipate heat generated within the stack and helps to suppress flux jumping. By cutting and stacking HTS tapes, Patel *et al*. produced a captured magnetic field of 17.7 T at a temperature of 8 K in 2018 [13], demonstrating that engineering current density comparable to bulk superconductors can be achieved in stacked HTS tapes.

In this paper, we designed magnetic lenses based on HTS tapes for high-field, up to 20 T, applications. We implemented numerical simulations to compare various magnetic lenses with different topologies of HTS stacks. The influences of the geometric design on the concentration effect and the related mechanism have been systematically investigated.

## II. Details of the Numerical Model

The numerical simulations based on the H-$\phi$ formulation [14] were implemented using the finite element software COMSOL Multiphysics. The H-$\phi$ formulation is a hybrid formulation combining the magnetic field strength $\mathbf{H}$ in the superconducting region and the magnetic scalar potential $\phi$ in the nonconducting region. Arsenault *et al*. showed that for some uncomplicated geometries, the H-$\phi$ formulation could significantly improve the computational speed and obtain solutions with the same accuracy compared to the H-formulation [15], [16].

The governing formulation in the conductive area, combining Ampere's law and Faraday's law, is the same as the H-formulation [17], [18]:

$$\nabla \times \mathbf{H} = \mathbf{J} \tag{1}$$

$$\nabla \times \mathbf{E} = -\frac{\partial \mathbf{B}}{\partial t} \tag{2}$$

This work was supported in part by National Key Research and Development Program (2016YFF0101701), the Strategic Priority Research Program of Chinese Academy of Sciences (XDB25000000), and the project (6140923050202). M.D. Ainslie was supported by the Engineering and Physical Sciences Research Council (EPSRC) Early Career Fellowship, EP/P020313/1. All data are provided in full in the results section of this paper. (Corresponding author: Difan Zhou.)

Wenhao Li, Qing Zhang, Difan Zhou, Jinyu He, Yibing Zhang, and Chuanbing Cai are with the Shanghai Key laboratory of High Temperature Superconductors, Shanghai University, Shanghai 200444, China (e-mail: dz286@shu.edu.cn).

M.D. Ainslie is with the Bulk Superconductivity Group, Department of Engineering, Cambridge CB2 1PZ, UK (e-mail: mark.ainslie@eng.cam.ac.uk).

Color versions of one or more of the figures in this paper are available online at http://ieeexplore.ieee.org.

Digital Object Identifier will be inserted here upon acceptance.

$$\nabla \times (\rho \nabla \times \mathbf{H}) = -\mu_0 \frac{\partial \mathbf{H}}{\partial t} \quad (3)$$

where $\rho$ is the resistivity and $\mu_0$ is the magnetic permeability of air. The *E-J* power law [19], [20] is used to simulate superconducting nonlinear resistivity:

$$\rho = \frac{E_c}{J_c(B)} \left| \frac{\mathbf{J}}{J_c(B)} \right|^{n-1} \quad (4)$$

where $\mathbf{J}$ is the current density, $J_c(B)$ is the field-dependent critical current density, $E_c$=$10^{-4}$ V/m, and n=21 is assumed as a reasonable approximation for HTS materials [21], [22]. We used the $J_c(B)$ data at 4.2 K reported for Superpower's HTS tape from its official website. We fitted and extended the measured results using equation (5) [23], [24]:

$$J_c(B) = J_{c0}/(1 + \frac{B}{B_0})^{\alpha} \quad (5)$$

and the fitting parameters for $J_{c0}$, $B_0$, and $\alpha$ are $6.17\times10^{11}$ A/m$^2$, 0.47 T, and 0.72, respectively. The HTS tape used in the simulation has a total thickness of 34 μm, the superconducting layer is 1 μm, and the homogenization model is used to simplify the complex layered structure of the HTS tape [25], [26]. Taking into account the anisotropy of the HTS tape, the following formula is used for the calculation [27]-[30]:

$$J_c(B) = \frac{J_{c0}}{\left(1+\frac{\sqrt{k^2|B_\parallel|^2+|B_\perp|^2}}{B_0}\right)^{\alpha}} \quad (6)$$

where $k$ is a factor characterizing the anisotropy of the HTS material, which is 0.295, and other parameters were the same as above. Ampere's law indicates that $\nabla \times \mathbf{H} = 0$ when the displacement current is neglected in the non-superconducting domains. According to Gauss's law, $\nabla \cdot \mathbf{B} = 0$, combined with $\mathbf{H} = -\nabla\phi$ and $\mathbf{B} = \mu_0\mu_r\mathbf{H}$, the governing equation of the non-conductive domains can be obtained as follows:

$$\nabla \cdot \nabla\phi = 0 \quad (7)$$

Isothermal conditions are assumed since the magnetization process is very slow. Therefore, the simulation does not include the thermal model [31]. Due to the geometric symmetry of the magnetic lens, only one part of the model needs to be simulated to give accurate results of the entire model and significantly speed up the simulation.

## III. Results and Discussion

### A. Rectangular-shaped magnetic lens and its optimization

Firstly, we studied the rectangular-shaped magnetic lens constructed using two stacks of HTS tapes. We investigated the influence of the stack height $H$, tape width $D$, and stack spacing $S$ on the concentration effect using a 2D model, and discussed the additional dimension, the length of the HTS tapes, using a 3D model.

Fig. 1 shows the influence of these geometric parameters on the central magnetic flux density $B_c$ of the magnetic lens when $B_{app}$ = 20 T and $T$ = 4.2 K. Fig. 1(a) shows that $B_c$ reaches the maximum value of 22.79 T at $H$=11.9 mm, and the magnetic field amplification coefficient $B_c/B_{app}$ also reaches the maximum value indicating that the magnetic lens has an optimal aspect ratio. The value of $B_c$ increases linearly with increasing $D$ and decreasing $S$, as shown in Fig. 1(b) and Fig.1(c). In Fig. 1(d), the value of $B_c$ increases nonlinearly as $L$ increases. $B_c$ reaches 22.69 T when $L$ = 72 mm corresponding to a gain factor greater than 20%. $B_c$ tends to be saturated at around 22.79 T when $L$ keeps increasing.

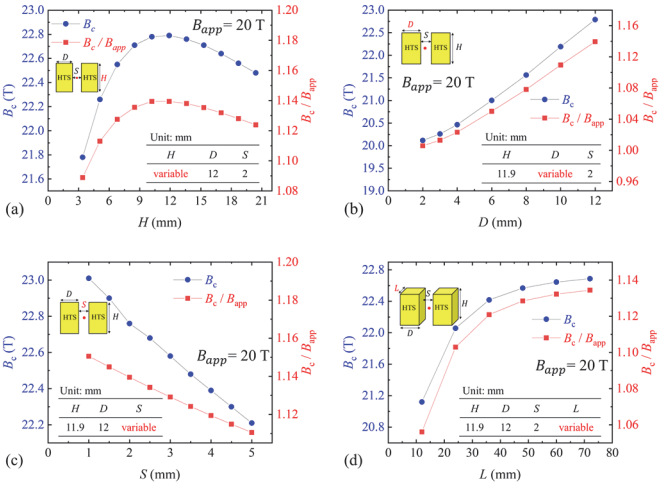


Fig. 1. When $B_{app}$ = 20 T, the effects of changing (a) $H$, (b) $D$, (c) $S$, and (d) $L$ on $B_c$ and $B_c/B_{app}$.

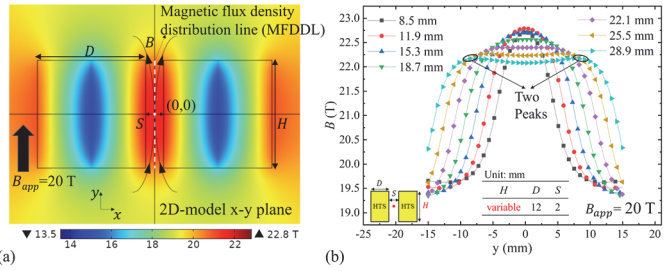


Fig. 2. (a) Magnetic flux density distribution on the XY plane of the 2D rectangular-shaped magnetic lens ($S$=2 mm, $D$=12 mm, $H$=11.9 mm) and the magnetic flux density distribution line (MFDDL). (b) The effect of changing $H$ on the magnetic flux density distribution on MFDDL.

Fig. 2 shows the magnetic flux density distribution of the 2D rectangular-shaped magnetic lenses along the central line parallel to the Y-axis, indicated by a white dashed line in Fig. 2(a) and is named the magnetic flux density distribution line (MFDDL). The applied $B_{app}$ is parallel to the Y-axis. We take the two endpoints of MFDDL as (0,15) and (0, -15). Fig. 2(b) shows that the value of $B_c$ initially increases and then decreases with $H$, and reaches the maximum value at $H$ =11.9 mm. Meanwhile, the concentration area enlarges with the increasing $H$. The central peak gradually evolved into two shoulders as indicated by two black circles on the curve of $H$=28.9 mm in fig. 2(b).

Fig. 3 compares the magnetic flux concentration ability of three different 3D magnetic lenses with applied $B_{app}$ parallel to the Z-axis. To obtain a larger central magnetic flux density, we designed a magnetic lens composed of four stacks of tapes namely the petal-shaped magnetic lens and a magnetic lens made by partially slotting a stack of wide tapes, as shown in the middle and right of Fig. 3(a). The general idea is to enlarge the shielding areas to enhance the central magnetic field.

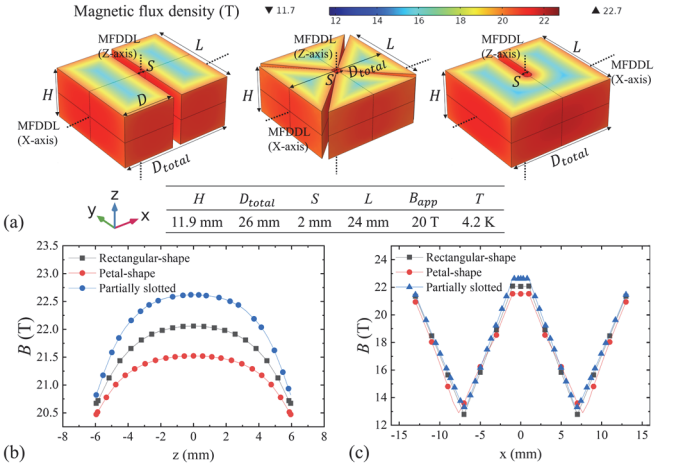


Fig. 3. (a) The magnetic flux density distribution of the superconducting part of the rectangular-shaped magnetic lens, the petal-shaped magnetic lens, and the partially slotted magnetic lens at $B_{app}$=20 T, respectively. (b) Magnetic flux density distribution of the three models on the same Z-axis direction MFDDL. (c) Magnetic flux density distribution of the three models on the same X-axis direction MFDDL.

We made an MFDDL parallel to the Z-axis with two endpoints at (0, 0, 5.95) and (0, 0, -5.95) respectively, to compare the magnetic flux concentration effects of different magnetic lenses as shown in Fig. 3(b). It can be found that the $B_c$ of the petal-shaped magnetic lens is smaller than that of the rectangular-shaped magnetic lens. This is caused by the small tape size which greatly restricted the induced shielding current loop. For the partially slotted magnetic lens, we used the 26 mm wide HTS tape which is commercially available, and cut a 2 mm wide slit to the center of the stack. Such a magnetic lens yields a higher $B_c$ than that of the rectangular-shaped magnetic lens due to a larger induced current loop and hence a much stronger diamagnetic shielding ability.

Fig 3(c) shows the distribution of magnetic flux density along the MFDDL in the X-axis direction for the three types of magnetic lenses. The two endpoints are (-13, 0, 0) and (13, 0, 0) as noted by the dashed line in Fig. 3(a). The results show that the magnetic flux density is significantly uniform in the gap which is designed as the magnetic flux concentration zone.

### *B. X-shaped magnetic lens and its optimization*

Kiyoshi *et al*. have demonstrated the concept of magnetic flux concentration using funnel-shaped superconducting bulks. Similarly, we designed the X-shaped magnetic lens suing HTS tapes. We investigated the geometric parameters of the stacking spacing $S$, the tape width $D$, the height $H1$ of the non-inclined part, the height $H2$ of the inclined part, and the angle $\theta$ between the inclined part and the horizontal direction using a 2D model, and discuss the length $L$ based on a 3D model.

Fig. 4 summarizes the influence of these geometric parameters on the magnetic flux concentration effect of the X-shaped magnetic lens under the conditions of $B_{app}$=20 T and $T$=4.2 K. Fig. 4(a) shows the magnetic flux density distribution of the 2D X-shaped model and the MFDDL to be studied. As shown in Fig. 4(b) and 4(c), $B_c$ increases with decreasing $S$ or increasing

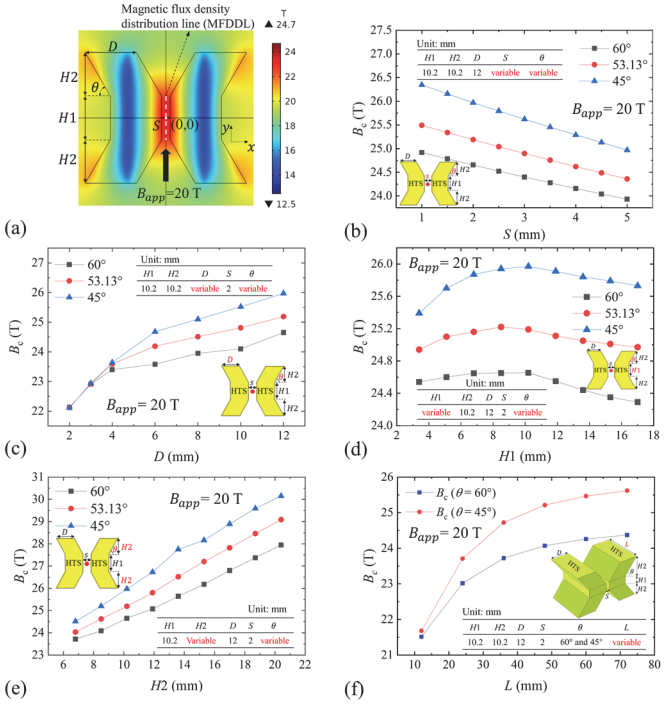


Fig. 4. (a) Magnetic flux density distribution diagram and geometric parameters to be discussed for a 2D X-shaped magnetic lens when $B_{app}$ =20 T ($H1$=$H2$=10.2 mm, $D$=12 mm, $S$=2 mm, $\theta$=60°). (b), (c), (d), and (e) The variations of $B_c$ with $S$, $D$, $H1$, and $H2$ at different angles $\theta$ in the 2D models, respectively. (f) The relationship between $B_c$ and the tape length $L$ of the 3D model for $\theta$=60° and 45°.

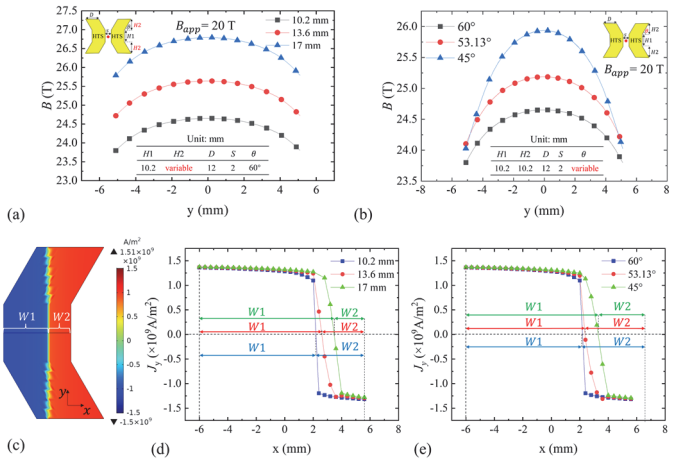


Fig. 5. (a) and (b) Magnetic flux density on the MFDDL in the Y-axis direction when changing the $H2$ and $\theta$ of the 2D X-shaped magnetic lens, respectively. (c) Induced current density distribution of the 2D X-shaped magnetic lens ($H1$=$H2$=10.2 mm, $D$=12 mm, $S$=2 mm, $\theta$=60°). (d) and (e) Induced current density distribution along the X-axis for different $H2$ and $\theta$, respectively.

$D$. Fig. 4(d) shows that there is an optimal value of $H1$ that maximizes $B_c$. Fig. 4(e) shows that $B_c$ increases linearly with the increase of $H2$. It can as well be concluded that $B_c$ increases with decreasing $\theta$ when the other parameters are fixed. Fig. 4(f)

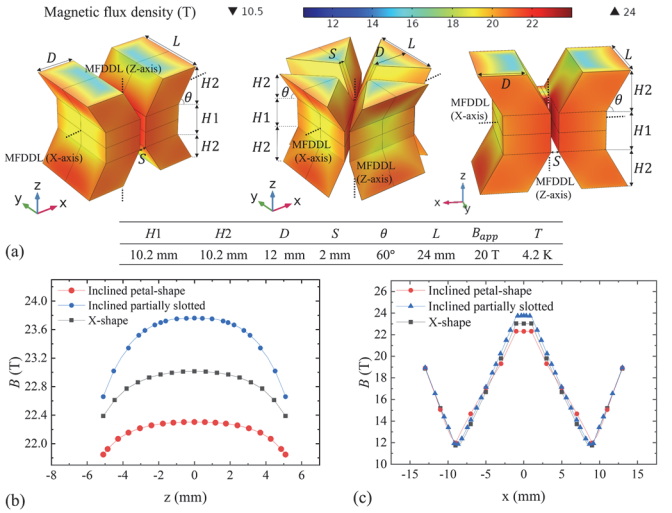


Fig. 6. (a) Magnetic flux density distribution for the 3D X-shaped magnetic lens, the inclined petal-shaped magnetic lens, and the inclined partially slotted magnetic lens, respectively. (b) Magnetic flux density distribution on MFDDL in the Z-axis direction for the three different models. (c) Magnetic flux density distribution on the MFDDL in the X-axis direction for the three different models.

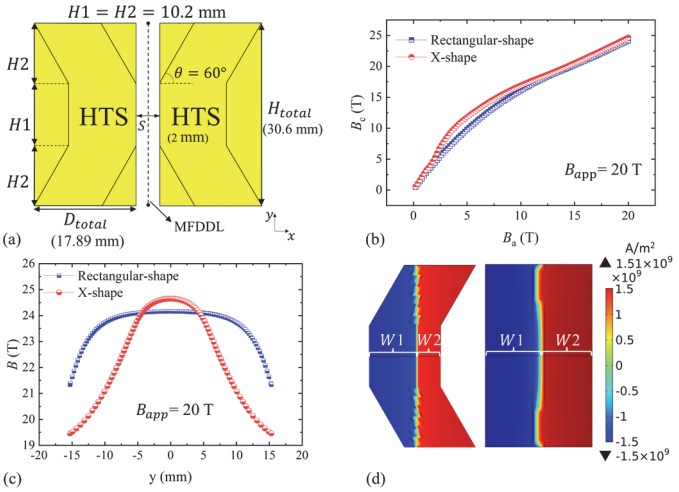


Fig. 7. (a) The shape of 2D rectangular-shaped and X-shaped magnetic lens of the same size. (b) The $B_c$ of the rectangular-shaped and X-shaped magnetic lens varies with $B_{app}$. (c) The magnetic flux density distribution of the rectangular-shaped and X-shaped magnetic lenses on the Y-axis MFDDL. (d) The induced current density of rectangular-shaped and X-shaped magnetic lenses.

shows that $B_c$ increases nonlinearly with $L$ and tends to saturate. After optimizing the topology of the 3D X-shaped magnetic lens, $B_c$ of 25.62 T can be achieved with $\theta$=45° and $L$=72 mm, corresponding to an enhancement of more than 25%.

Fig. 5(a) and (b) show the magnetic flux density on the MFDDL (white dashed line shown in Fig.4a) of the 2D model with $B_{app}$ parallel to the Y-axis. A smaller $\theta$ and a larger $H2$ yield a higher magnetic field on the MFDDL.

Fig. 5(c) shows the distribution of the current density on the cross section of half of the 2D X-shaped magnetic lens. Apparently, the current flows inward and outward to the paper is uneven in the non-inclined part which can be expressed as the ratio between W1 and W2. A greater W1/W2 ratio leads to a better concentration effect at the central area. It can be seen that as $H2$ increases or $\theta$ decreases, the W1/W2 ratio enlarges as shown in Fig. 5(d) and (e) respectively.

In order to optimize the X-shaped magnetic lens, we further developed the 3D petal-shaped and partially slotted magnetic lenses to add inclined parts, as shown in Fig. 6(a). Fig. 6(b) and (c) compares the magnetic flux concentration effects of these three models and shows a good uniformity of the magnetic flux density along the X-axis direction at the concentrated area. Similar results have been achieved that the $B_c$ of the petal-shaped magnetic lens is relatively smaller while the partially slotted magnetic lens exhibits a better concentration effect.

### *C. Comparison of rectangular-shaped magnetic lens and X-shaped magnetic lens*

Fig. 7 compares the magnetic flux density concentration effects of the rectangular-shaped model and the X-shaped model when $B_{app}$=20 T and $T$=4.2 K. We assume they have the same $H_{total}$ and $D_{total}$, as shown in Fig.7(a). Fig. 7(b) shows the variation of $B_c$ with $B_{app}$ of the two models. The X-shaped model can obtain a larger $B_c$. Fig. 7(c) shows the $B$ values of the two lenses on the MFDDL with endpoints (0, 15.3) and (0, -15.3), respectively. Fig. 7(d) shows that for the X-shaped model, the width ratio $W1/W2$ in the non-tiled area is significantly larger than that in the rectangular-shaped model. This explains the reason why the X-shaped magnetic lens can concentrate magnetic fluxes more effectively.

## IV. CONCLUSION

In this paper, we have designed and simulated stacked-tape magnetic lenses using 2D and 3D models based on the H-$\phi$ formulation. The optimized topologies of stacks that contribute to the concentration of magnetic flux density have been obtained. Central magnetic fields of 22.69 T and 25.62 T have been achieved with the rectangular-shaped and X-shaped magnetic lenses respectively under an external magnetic field of 20 T. The X-shaped magnetic lens yields a greater central magnetic field compared with the rectangular magnetic lens. This can be explained by the uneven screening current distribution in the tilted and non-tilted parts of the X-shaped model. We have further designed a magnetic lens by partially slotting a stack of 26 mm wide tapes. Such a magnetic lens shows a better concentration effect owning to a larger induced screening current loop. This passive device is considered a promising alternative component to increase the magnetic field in a compact high-field superconducting magnet.

## REFERENCES


[1] S. Choi, T. Kiyoshi, and S. Matsumoto, "Magnetic field amplifier employing high-Tc bulk superconductor," *J. Appl. Phy.,* vol. 105, no. 7, 2009, Art. no. 07E705.

[2] S. Choi, J. H. Yoon, B. S. Lee *et al.*, "Magnetic lens effect using Gd-Ba-Cu-O bulk superconductor in very high magnetic field," *J. Appl. Phys.,* vol. 111, no. 7, 2012, Art. no. 07E728

[3] T. Kiyoshi, S. Choi, S. Matsumoto *et al.*, "Magnetic Flux Concentrator Using Gd-Ba-Cu-O Bulk Superconductors," *IEEE Trans. Appl. Supercond.,* vol. 19, no. 3, pp. 2174-2177, 2009.

[4] S. Matsumoto, T. Asano, T. Kiyoshi *et al.*, "Magnetic flux concentration using YBCO hollow and solid cylinders," *IEEE Trans. Appl. Supercond.,* vol. 14, no. 2, pp. 1666-1669, Jun. 2004.

[5] Z. Y. Zhang, S. Matsumoto, R. Teranishi *et al.*, "Magnetic field, temperature and mechanical crack performance of a GdBCO magnetic lens," *Supercond. Sci. Technol.,* vol. 25, no. 11, Nov. 2012, Art. no. 115012.

[6] Z. Y. Zhang, S. Matsumoto, R. Teranishi *et al.*, "Improving the properties of GdBCO magnetic lenses by adopting a new design and resin impregnation," *Supercond. Sci. Technol.,* vol. 26, no. 4, Apr. 2013, Art. no. 045001.

[7] S. Namba, H. Fujishiro, M. D. Ainslie *et al.*, "Design Optimization of a Hybrid Trapped Field Magnet Lens (HTFML)," *IEEE Trans. Appl. Supercond.,* vol. 29, no. 5, Aug. 2019, Art. no. 6801605.

[8] S. Namba, H. Fujishiro, T. Hirano *et al.*, "Optimized performance of an all-REBaCuO hybrid trapped field magnet lens (HTFML) with liquid nitrogen cooling," *Physica C: Supercond.,* vol. 575, Aug. 2020, Art. no.1353690.

[9] S. Namba, H. Fujishiro, T. Naito *et al.*, "Experimental realization of a hybrid trapped field magnet lens using a GdBaCuO magnetic lens and MgB2 bulk cylinder," *Supercond. Sci. Technol.,* vol. 32, no. 12, Dec. 2019, Art. no. 12LT03.

[10] K. Takahashi, H. Fujishiro, and M. D. Ainslie, "A new concept of a hybrid trapped field magnet lens," *Supercond. Sci. Technol.,* vol. 31, no. 4, Apr. 2018, Art. no. 044005.

[11] K. Takahashi, H. Fujishiro, and M. D. Ainslie, "Simulation study for magnetic levitation in pure water exploiting the ultra-high magnetic field gradient product of a hybrid trapped field magnet lens (HTFML)," *J. Appl. Phys.,* vol. 127, no. 18, May. 2020, Art. no. 185106.

[12] K. Takahashi, H. Fujishiro, S. Namba *et al.*, "Experimental realization of an all-(RE)BaCuO hybrid trapped field magnet lens generating a 9.8 T concentrated magnetic field from a 7 T external field," *Supercond. Sci. Technol.,* vol. 34, no. 5, Apr. 2021, Art. no. 05LT02.

[13] A. Patel, A. Baskys, T. Mitchell-Williams *et al.*, "A trapped field of 17.7 T in a stack of high temperature superconducting tape," *Supercond. Sci. Technol.,* vol. 31, no. 9, 2018, Art. no. 09LT01.

[14] A. Arsenault, F. Sirois, and F. Grilli, "Implementation of the H-ϕ Formulation in COMSOL Multiphysics for Simulating the Magnetization of Bulk Superconductors and Comparison With the H-Formulation," *IEEE Trans. Appl. Supercond.,* vol. 31, no. 2, Mar. 2021, Art. no. 6800111.

[15] A. Arsenault, B. d. S. Alves, and F. Sirois, "COMSOL Implementation of the H-ϕ-Formulation With Thin Cuts for Modeling Superconductors With Transport Currents," *IEEE Trans. Appl. Supercond.,* vol. 31, no. 6, pp. 1-9, Sep. 2021, Art. no. 6900109.

[16] A. Arsenault, F. Sirois, and F. Grilli, "Efficient Modeling of High-Temperature Superconductors Surrounded by Magnetic Components Using a Reduced H–ϕ Formulation," *IEEE Trans. Appl. Supercond.,* vol. 31, no. 4, pp. 1-9, Jun. 2021, Art. no. 6800609.

[17] B. Y. Shen, F. Grilli, and T. Coombs, "Review of the AC loss computation for HTS using H formulation," *Supercond. Sci. Technol.*, vol. 33, no. 3, Mar, 2020, Art. no. 033002.

[18] B. Y. Shen, F. Grilli, and T. Coombs, "Overview of H-Formulation: A Versatile Tool for Modeling Electromagnetics in High-Temperature Superconductor Applications," *IEEE Access*, vol. 8, pp. 100403-100414, 2020.

[19] C. Plummer, and J. Evetts, "Dependence of the shape of the resistive transition on composite inhomogeneity in multifilamentary wires," *IEEE Trans. Magn.,* vol. 23, no. 2, pp. 1179-1182, 1987.

[20] J. Rhyner, "Magnetic properties and AC-losses of superconductors with power law current—voltage characteristics," *Physica C: Supercond.,* vol. 212, no. 3-4, pp. 292-300, 1993.

[21] F. Grilli, S. Stavrev, Y. Le Floch *et al.*, "Finite-element method modeling of superconductors: From 2-D to 3-D," *IEEE Trans. Appl. Supercond.,* vol. 15, no. 1, pp. 17-25, Mar, 2005.

[22] M. Zhang, and T. A. Coombs, "3D modeling of high-Tc superconductors by finite element software," *Supercond. Sci. Technol.,* vol. 25, no. 1, Dec. 2011, Art. no. 015009.

[23] P. W. Anderson, "Theory of Flux Creep in Hard Superconductors," *Phys. Rev. L.,* vol. 9, no. 7, pp. 309-311, 1962.

[24] N. Nibbio, S. Stavrev, and B. Dutoit, "Finite Element Method simulation of AC loss in HTS tapes with B-dependent E-J power law," *IEEE Trans. Appl. Supercond.,* vol. 11, no. 1, pp. 2631-2634, Mar. 2001.

[25] Z. Hong, and T. A. Coombs, "Numerical Modelling of AC Loss in Coated Conductors by Finite Element Software Using H Formulation," *J Supercond. Nov Magn.,* vol. 23, no. 8, pp. 1551-1562, Dec. 2010.

[26] V. M. R. Zermeno, A. B. Abrahamsen, N. Mijatovic *et al.*, "Calculation of alternating current losses in stacks and coils made of second generation high temperature superconducting tapes for large scale applications," *J. Appl. Phys.,* vol. 114, no. 17, Nov. 2013, Art. no. 173901.

[27] F. Gomory, M. Vojenciak, E. Pardo *et al.*, "AC losses in coated conductors," *Supercond. Sci. Technol.,* vol. 23, no. 3, Mar. 2010, Art. no. 034012.

[28] E. Pardo, M. Vojenciak, F. Gomory *et al.*, "Low-magnetic-field dependence and anisotropy of the critical current density in coated conductors," *Supercond. Sci. Technol.,* vol. 24, no. 6, Jun. 2011, Art. no. 065007.

[29] J. Šouc, E. Pardo, M. Vojenčiak *et al.*, "Theoretical and experimental study of AC loss in high temperature superconductor single pancake coils," *Supercond. Sci. Technol.,* vol. 22, no. 1, 2009, Art. no. 015006.

[30] M. Vojenčiak, F. Grilli, S. Terzieva *et al.*, "Effect of self-field on the current distribution in Roebel-assembled coated conductor cables," *Supercond. Sci. Technol.,* vol. 24, no. 9, 2011, Art. no. 095002.

[31] M. D. Ainslie, A. Yamamoto, H. Fujishiro *et al.*, "Numerical modelling of iron-pnictide bulk superconductor magnetization," *Supercond. Sci. Technol.,* vol. 30, no. 10, Oct. 2017, Art. no. 105009.